


## Generation of subcycle isolated attosecond pulses by pumping ionizing gating

Zhaohui Wu <sup>\*</sup>, Xiaoming Zeng, Zhaoli Li, Zhimeng Zhang, Xiaodong Wang, Xiao Wang, Jie Mu, Yanlei Zuo,<sup>†</sup> and Jingqin Su  
National key laboratory of plasma physics, Research Center of Laser Fusion, China Academy of Engineering Physics,  
Mianyang, Sichuan, China, 621900.

Hao Peng<sup>\*</sup>

College of Physics and Optoelectronic Engineering, Shenzhen University, Shenzhen 518060, China

Huabao Cao  and Yuxi Fu

Center for Attosecond Science and Technology, Xi'an Institute of Optics and Precision Mechanics, Chinese Academy of Sciences, Xi'an  
710119, Shaanxi, China

C. Riconda

LULI, Sorbonne Université, CNRS, École Polytechnique, CEA, F-75005, Paris, France

S. Weber

ELI Beamlines facility, Extreme Light Infrastructure ERIC, 25241 Dolni Brezany, Czech Republic



(Received 28 July 2023; accepted 8 January 2024; published 31 January 2024)

We present an interesting approach named as pumping ionizing gating (PIG) for the generation of isolated attosecond pulses (IAPs). In this regime, a short laser is used to ionize a preexisting gas grating, creating a fast-extending plasma grating (FEPG) having an ionization front propagating with the velocity of light. A low-intensity long counterpropagating pump pulse is then reflected by a very narrow region of the ionization front, only where the Bragg conditions for resonant reflection is satisfied. Consequently, the pump reflection is confined within a subcycle region called PIG, and forms a wide-band coherent IAP in combination with the frequency up-conversion effect due to the plasma gradient. This approach results in a new scheme to generate IAPs from long picosecond pump pulses. Three-dimensional (3D) simulations show that a 1.6 ps, 1  $\mu\text{m}$  pump pulse can be used to generate a 330 as laser pulse with a peak intensity approximately 33 times that of the pump and a conversion efficiency of around 0.1%. These results highlight the potential of the PIG method for generating IAPs with high conversion efficiency and peak intensity.

DOI: [10.1103/PhysRevResearch.6.013126](https://doi.org/10.1103/PhysRevResearch.6.013126)

### I. INTRODUCTION

Ultrafast techniques have enabled the generation of laser pulses with durations on the attosecond scale, allowing for the direct observation of electron motion in various systems such as atoms, molecules, and solids. Isolated attosecond pulses (IAPs) are typically generated through gas high harmonics generation (GHHG) with gating techniques [1–23], which have spectral coverage from hard x-rays to extreme ultraviolet (EUV, <120 nm) and durations as short as a few tens of attoseconds. However, the pulse energies of these IAPs are limited to the nanojoule range due to the low efficiency of

high harmonics generation. Alternative methods for generating IAPs include coherent field synthesis [24–26], which has been demonstrated to produce pulses with durations of as short as 380 attoseconds and spectra covering the deep ultraviolet to near infrared range [25]. It leads to longer pulse durations while allowing for higher pulse energies (tens of microjoules). Further increasing of the IAPs energy opens new possibilities for the nonlinear attosecond optics. However, it is limited by the energy of the few-cycle driving pulses.

The key principle behind GHHG for generating IAPs lies in the use of gating techniques to confine the resonant generation zone to a narrow temporal region. However, this inherently results in low energy transfer efficiency since a significant portion of the driving pulse is not utilized. On the other hand, plasma has been shown to be an effective media for laser compression by exploiting the plasma waves [27–39] or fast-extending plasma grating (FEPG) [40,41]. This technique enables laser compression with high peak power and efficiency. However, the shortest duration of the output pulse is limited to several optical cycles. In this paper, we propose an interesting approach to making joule-level IAPs possible

<sup>\*</sup>These authors contribute equally to this work.

<sup>†</sup>zuoyanlei@tsinghua.org.cn

Published by the American Physical Society under the terms of the [Creative Commons Attribution 4.0 International](https://creativecommons.org/licenses/by/4.0/) license. Further distribution of this work must maintain attribution to the author(s) and the published article's title, journal citation, and DOI.

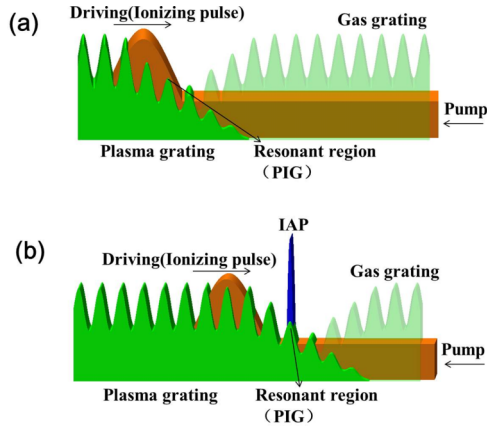


FIG. 1. (a) Illustration of the pumping ionizing gating (PIG) formed by the gradient FEPG. (b) Scheme of IAP generation due to pump reflection and frequency upconversion in the resonant region (PIG).

by incorporating ionization gating techniques into the plasma compression using a gradient FEPG. The FEPG is formed by utilizing a short laser pulse to ionize a background gas grating, which can be created using established methods such as stimulated Brillouin scattering (SBS) [40–46] or interference ionization [47] in the gas medium. Following the ionization pulse, the plasma grating has a boundary extending at the light speed. In previous studies, the pump beam is resonantly reflected in the bulk plasma grating region to ensure pump depletion [40,41]. However, in our proposed scheme, as illustrated in Fig. 1(a), the resonant reflection region of the pump is confined to a narrow region at the ionization front by selecting a proper grating period. Within this ionization front, the gas grating is gradually ionized by the driving pulse, resulting in an increasing average plasma density  $n_{e0}\rho(\xi)$ , where  $\xi = z - tv_g$ ,  $v_g$  is the group velocity of the driving pulse,  $\rho$  is the ionization rate, and  $n_{e0}$  is average electron density of the fully ionized gas. For a grating with a period  $\Lambda$ , the Bragg condition for resonant reflection of the pump can only be fulfilled in a very narrow region around  $\xi \approx \xi_0$ , given by  $k_0 N_0 \Lambda = \pi$ , where  $k_0 = 2\pi/\lambda_0$  and  $\lambda_0$  are the pump wave vector and wavelength, and  $N_0 = (1 + \sqrt{1 - n_{e0}\rho(\xi_0)/n_c})/2$  represents the refractive index at the resonant region of the FEPG [41]. Moreover, as the laser propagates through the gradient plasma, a frequency-upconversion effect occurs [48–52]. Consequently, the reflected pump beam is confined and upconverted in the narrow resonant region, resulting in a wide-band coherent IAP, as shown Fig. 1(b). Since the reflected pulse extracts energy from the entire long pump pulse, we call the approach pumping ionizing gating (PIG) which enables the IAP energy several orders of magnification higher than the present level.

## II. THEORETICAL MODEL

To explain the physical model of PIG, we first consider the energy transfer from the pump to driving pulse by the FEPG, which is given by the coupled-waves equation in the variable

of  $\xi$  [40]:

$$\begin{aligned} \frac{\partial E}{\partial t} &= -i \frac{\omega_{pe}^2}{2\omega_0} E_0 f e^{2i\omega_0 \delta N t}, \\ &\times \frac{\partial E_0}{\partial t} - 2v_g \frac{\partial E_0}{\partial \xi} = -i \frac{\omega_{pe}^2}{2\omega_0} E f e^{-2i\omega_0 \delta N t}, \end{aligned} \quad (1)$$

where  $E$  and  $E_0$  are the electric field of driving pulse and pump pulse, respectively,  $\omega_{pe} = \sqrt{n_e e^2 / m_e \epsilon_0}$  is the plasma frequency,  $n_e$  is the electron density,  $e$  and  $m_e$  are the electron charge and mass,  $\epsilon_0$  is the permittivity,  $f \equiv \frac{\delta n_{e0}}{n_{e0}}$  is the normalized FEPG amplitude,  $\delta n_{e0}$  is the amplitude of the fully ionized plasma grating, and  $\omega_0$  is the pump frequency.

The electron density  $n_e$  in the gradient FEPG can be written as

$$n_e = \begin{cases} n_{e0} + \delta n_{e0} \sin(2\pi \xi / \Lambda), & \xi < -L, \\ \rho [n_{e0} + \delta n_{e0} \sin(2\pi \xi / \Lambda)], & -L \leq \xi \leq 0, \\ 0, & \xi > 0, \end{cases} \quad (2)$$

where  $L$  is the length of the ionization front.

As most regions of the gradient FEPG can not satisfy the resonant condition, there is a detuning factor of  $e^{2i\omega_0 \delta N t}$  in Eq. (A3), where  $\delta N = (N - N_0)$ ,  $N = (1 + \sqrt{1 - \rho(\xi) n_{e0} / n_c})/2$  is the refractive index of the pump in FEPG [41], and  $n_c = \omega_0^2 m_e \epsilon_0 / n_{e0} e^2$  is the critical plasma density for the pump. One has  $2k_0 N_0 \Lambda = 2\pi$ , therefore

$$\Lambda = \lambda_0 / (1 + \sqrt{1 - \rho(\xi_0) n_{e0} / n_c}). \quad (3)$$

From Eqs. (A3) and (3) it can be seen that the growth rate of the driving pulse decreases exponentially at the position away from the resonant point, therefore a narrow gating is created, and it moves to the position of higher  $\rho$  as  $\Lambda$  increases. For  $\rho = 1$ , Eq. (3) becomes the standard Bragg condition of FEPG [41].

In a medium with a time-varying refractive index, the laser experiences a frequency shift while maintaining a constant wave vector in order to satisfy the dispersion relation [51]. Theoretical models have been developed to describe this phenomenon in the ionizing plasma [48–50]. In the case of the ionizing plasma grating, although the periodic structure also provides a time-varying refractive index, the integration over one period is close to zero. Consequently, the frequency upconversion effect resulting from the grating structure can be neglected, allowing us to extend the existing theoretical models to the gradient FEPG. To validate this assumption, we performed particle-in-cell (PIC) simulations using the same laser pulse to ionize the gas and the gas grating. The upconverted spectra were found to be nearly identical (see Fig. 6).

For a laser-induced plasma, a roughly linear density gradient is formed in the pulse front. The upconverted light has an analytical solution of  $\frac{\omega_0}{\omega} E e^{i\omega t (\xi - \xi_0)}$  when  $\omega_{pe} \ll \omega$ , where  $\omega = \omega_0 (1 + ct \omega_{pe}^2 / L \omega_0^2)^{1/2}$  is the shifted laser frequency. However, the upconversion process in PIG is more complex due to the reflected pump. As the reflected pump is mainly affected by the plasma gradient and the propagation time, it can be approximately divided into a series of independent infinitesimal pulses. For  $dE$  at time  $t$ , the upconverted

TABLE I. Optimal parameters for the simulation of IAPs, where  $\lambda$ ,  $I$ ,  $\tau$ , and  $R$  are the laser central wavelength, peak intensity, FWHM duration, and beam waist, respectively,  $L_i$  is the length of gas grating.

Pump	$\lambda(\mu\text{m})$	$I(\text{W}/\text{cm}^2)$	$\tau(\text{ps})$	$R(\mu\text{m})$
Value	1	$4 \times 10^{13}$	1.6	50
Driving pulse	$\lambda(\mu\text{m})$	$I(\text{W}/\text{cm}^2)$	$\tau(\text{fs})$	$R(\mu\text{m})$
value	Arbitrary	$1 \times 10^{14}$	30	50
Gas grating	$n_{e0}(n_c)$	$\delta n_{e0}/n_{e0}$	$\Lambda(\mu\text{m})$	$L_i(\mu\text{m})$
Value	0.1	0.5	0.507	240

electric field at time  $t + \delta t$  can be described by

$$dE(t + \delta t) = \frac{\omega_0}{\omega(\delta t)} dE e^{i\omega(\delta t)(\xi - \xi_0)}. \quad (4)$$

As the resonant region in the gradient FEPG is very narrow, the pump reflectivity is small and  $E_0$  is approximate to a constant in Eq. (A3), so the driving pulse has an analytical solution by combing Eqs. (A3) and (4),

$$E = \int_0^t i \frac{\omega^2}{2\omega} E_0 f e^{2i\omega_0 \delta N t + i\omega(\xi - \xi_0)} dt. \quad (5)$$

The detailed derivation of Eq. (A7) is provided in Appendix A.

### III. PIC SIMULATION

In order to further visualize the mechanism, PIC simulations were carried out using the code EPOCH [53]. A picosecond pulse with intensity  $I_0 = 4 \times 10^{13} \text{ W}/\text{cm}^2$  and wavelength  $\lambda_0 = 1 \mu\text{m}$  was used as the pump. Temporally, it has a flat top and a 30 fs rising ramp, and the pulse duration is calculated by the interaction length of the pump and FEPG. A femtosecond Gaussian pulse with intensity  $10^{14} \text{ W}/\text{cm}^2$  and an arbitrary wavelength served as the driving (ionizing) pulse. In the 2D and 3D simulation, both the pump and driving pulse beams had a six-order super Gaussian transverse distribution with a beam waist of  $50 \mu\text{m}$ . The background gas grating was set to hydrogen with a modulation period near  $\sim \lambda_0/2$ . The ionization process was modeled using the Ammosov-Delone-Krainov tunnel ionization model [54].

We first show 3D PIC simulation with high efficiency energy transfer and generation of intense IAPs. Parametric scans of the plasma densities and groove depth allowed to identify the optimal result of IAPs (see Appendix B), and the optimal parameters are given in the Table I. In the simulation, a static window of  $200\lambda_0 \times 200\lambda_0$  for the transverse  $x$  and  $y$  directions and  $250\lambda_0$  for the longitudinal  $z$  direction was applied. Each cell had a size of  $\lambda_0 \times \lambda_0 \times \lambda_0/100$  and contained 16 particles. The output driving pulse has a FWHM duration of 330 as, and a peak intensity of  $\sim 33I_0$ , as shown in Fig. 2(c). The total conversion efficiency from the pump to the IAP is about 0.1%, which is only 1/7 of the 1D case. This is mainly due to the imperfect formation of IAPs at the beam edge where both the intensity of the input driving pulse and the pump decrease, as shown in Fig. 2(b). The simulation results suggest that the efficiency could be enhanced by employing a larger beam with a more uniform intensity distribution.

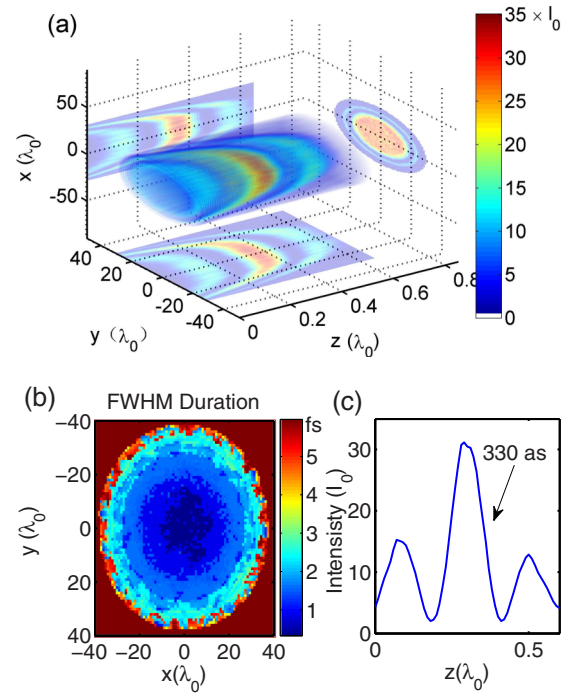


FIG. 2. (a) Profiles of the 3D IAPs. (b) Distribution of FWHM pulse duration. (c) Temporal intensity of the IAP at the beam center.

Varying the FEPG periods  $\Lambda$ , some typical features of PIG are observed as described below: First, the output driving pulse shifts toward regions of higher average density as  $\Lambda$  increases, with positions agreeing well with those of the resonant points predicted by Eq. (3), as demonstrated in Fig. 3(b) where several profiles of the driving pulses at different  $\Lambda$  are gathered together. Second, the pulse amplitude rises with  $\Lambda$ , mainly due to a stronger reflection of the pump at resonant regions with higher average density, as depicted in Fig. 3(b). Third, the pulse duration first swiftly decreases to attosecond and then increases again. As  $\Lambda$  increases, the PIG gradually forms, enabling the generation of IAPs within the range of  $0.504\lambda_0 \leq \Lambda \leq 0.507\lambda_0$ . However, when the resonant region is further shifted toward the fully ionized zone as  $\Lambda$  increases, the range becomes wider due to a smaller density gradient. Consequently, the pulse duration exhibits a rebound effect after achieving its shortest value, as depicted in Fig. 3(c). In experimental setups, the precise adjustment of  $\Lambda$  can be achieved by varying the incident angle of the pump. The frequency upconversion effect plays a significant role in the IAPs generation since it can provide a much wider spectrum for the output laser pulse. The PIC simulation shows that the central frequency of the IAP is shifted to around  $2\omega_0$  [see Fig. 3(d)], and the pulse duration changes to more than 100 fs with the frequency over  $1.8\omega_0$  absent, indicating the upconverted light is the key ingredient for IAPs. Moreover, we utilized the analytical model given by Eq. (A7) to investigate the influence of the upconversion effect while it cannot be explicitly removed in the PIC simulation. The analytical results with different  $\Lambda$  using Eq. (A7) with  $L = 8\lambda_0$  is presented in Figs. 3(d) and 3(e). They exhibit good agreement with the PIC simulation in terms of waveform profiles and pulse positions, and the central frequency of the IAP is also shifted

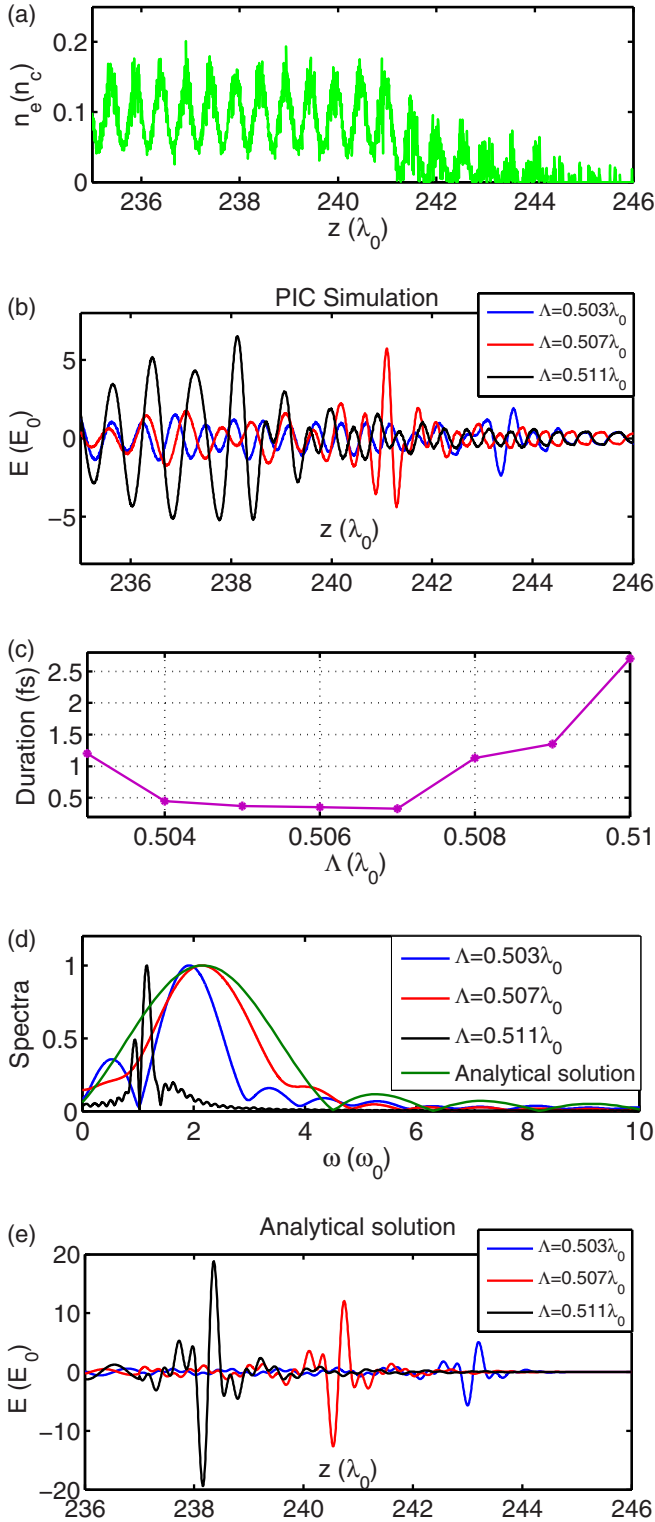


FIG. 3. (a) Distribution of the electron density in the gradient FEPG. (b) Electric field of the driving pulses at different  $\Lambda$  obtained by the PIC simulation. (c) The shortest durations (FWHM) of the driving pulse with various  $\Lambda$ . (d) Spectra of the driving-pulses at different grating periods, and the analytical solution. (e) Waveforms of the driving pulses at different  $\Lambda$  obtained by the analytical solution.

TABLE II. Summary of 1D PIC simulation results with various average plasma density ( $n_{e0}$ ) and modulation depths ( $\delta n_{e0}/n_{e0}$ ), where  $L_i$  is the interaction length,  $\tau$  is the FWHM duration of the driving pulse.

Case	I	II	III	IV	V	VI	VII
$n_{e0}(n_c)$	0.02	0.05	0.1	0.5	0.1	0.1	0.1
$\delta n_{e0}/n_{e0}$	0.5	0.5	0.5	0.5	0.1	0.2	0.6
$\Lambda$	0.5016	0.5035	0.507	0.535	0.506	0.506	0.507
$L_i(\text{mm})$	0.9	0.44	0.24	0.24	0.26	0.24	0.22
Peak $E(E_0)$	4.7	5.4	5.75	4.4	2.6	4.4	5.5
$\tau(\text{fs})$	0.42	0.38	0.33	0.32	0.42	0.4	0.35
efficiency(%)	0.15	0.39	0.7	1.3	0.14	0.48	0.72

to around  $2\omega_0$ . Note that the pulse spectra remains constant in the analytical model, whereas they vary in the PIC simulation with changing  $\Lambda$ . This discrepancy can be attributed to the assumption of a linear plasma gradient in the analytical model, whereas the PIC simulation incorporates a nonlinear gradient. Despite this difference, the analytical result can provide a qualitative investigation of the frequency upconversion effect. By disabling the upconversion effect in the analytical model, the pulse duration increases from hundreds of attoseconds to over 1 fs, implying that it is indispensable for IPAs.

PIG is available in a wide parameter range as it can be formed whenever any region along the gradient FEPG satisfies the resonant condition. To confirm this, we summarize the simulation results with different average densities and modulation depths in Table II (more details are given in Appendix B). The results show that IPAs can be obtained at a wide range of average plasma densities ( $0.02n_c$ – $0.5n_c$ ) and modulation depths ( $60\%n_{e0}$ – $10\%n_{e0}$ ). As shown in Table II, the required interaction length for IAP decrease with increasing average plasma density, indicating that higher plasma densities are preferred for higher conversion efficiency. However, the simulations reveal that pulse durations become unstable and peak intensities decrease when  $n_{e0} > 0.1n_c$ . Thus,  $n_{e0} = 0.1n_c$  is identified as the optimal plasma density. Furthermore, IPAs can still be generated at a modulation depth as small as  $10\%n_{e0}$ , indicating that the creation of the required gas grating for IPAs can be significantly simplified.

A sufficiently short input driving pulse is required to form a narrow resonant region. However, the pulse cannot be excessively short, or the resonant region would be less than one period, rendering it inefficient for forming a Bragg grating. In the PIC simulation, IPAs are obtained with the input pulse durations  $\tau_{in}$  ranging from 20 fs to 90 fs, as depicted in Fig. 4(a). The peak  $E$  first increases and then drops as  $\tau_{in}$  increases, with the maximum value of  $5.75E_0$  at  $\tau_{in} = 30$  fs. However, as shown in Eq. (A7) and Fig. 3(b), the peak  $E$  is also influenced by the grating period  $\Lambda$  which slightly varies with  $\tau_{in}$  to obtain optimal IPAs. Consequently, there is a dip of the peak  $E$  at  $\tau_{in}$  of 50–60 fs when  $\Lambda$  is relatively smaller, as shown in Fig. 4(b). In addition, a high contrast is not required, given that the peak intensity of the input driving pulse only

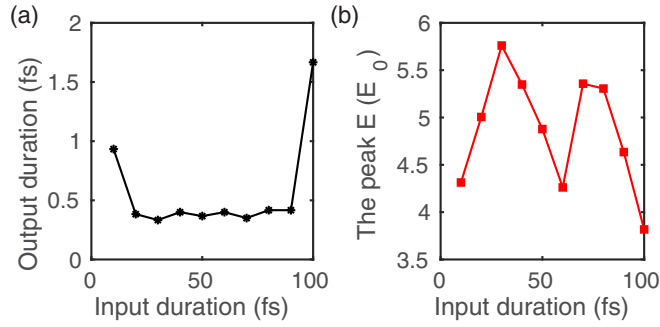


FIG. 4. Simulation results of the output FWHM duration  $\tau$  (a) and the peak  $E$  (b) of the driving pulse with various input FWHM durations  $\tau_{in}$ .

slightly surpasses the ionization threshold of the background gas (approximately  $10^{14}$  W/cm<sup>2</sup>). The requisite driving pulse can be readily provided by commercial Ti:sapphire CPA laser facilities.

#### IV. CONCLUSION

In summary, a method for generating IAPs, referred to as the PIG mechanism, has been proposed. This approach involves the reflection of a picosecond pump pulse by a gradient FEPG where a subcycle gating is formed in the narrow resonant region. In cooperation with the frequency upconversion effect of the laser in the gradient plasma, it allows for the generation of subcycle IAPs. The feasibility of the approach has been demonstrated through PIC simulations, showing that IAPs can be generated across a wide range of average plasma densities ( $0.02n_c$ – $0.5n_c$ ) and modulation depths ( $60\%n_{e0}$ – $10\%n_{e0}$ ). The 3D simulation results obtains a 330 as IAP in a 240  $\mu$ m long,  $0.1n_c$  density FEPG, with a conversion efficiency of  $\sim 0.1\%$ . Using a 1 kJ, 1.6 ps, 1053 nm laser pulse produced by chirped pulse amplification [55,56] as the pump would allow to generate joule-level IAPs.

#### ACKNOWLEDGMENTS

This work was partly supported by the Science and Technology on Plasma Physics Laboratory Fund (Grants No. 6142A04220203 and No. 6142A04220204)

#### APPENDIX A: ANALYTICAL SOLUTION

In order to understand the physical mechanism behind the pumping ionizing gating (PIG) process, we begin by examining the energy transfer from the pump pulse to the driving pulse via a fast-extending plasma grating (FEPG). This process can be described using the three-waves coupling equations for laser-plasma interaction [57]:

$$\begin{aligned} \left( \frac{\partial^2}{\partial t^2} - c^2 \Delta^2 + \omega_{pe}^2 \right) \mathbf{A} &= -\frac{4\pi e^2}{m_e} \delta n_e \mathbf{A}_0, \\ \left( \frac{\partial^2}{\partial t^2} - c^2 \Delta^2 + \omega_{pe}^2 \right) \mathbf{A}_0 &= -\frac{4\pi e^2}{m_e} \delta n_e \mathbf{A}, \\ \left( \frac{\partial^2}{\partial t^2} - c_s^2 \Delta^2 \right) \delta n_e &= \frac{Ze^2 n_{e0}}{m_e m_i c^2} \Delta^2 (\mathbf{A} \mathbf{A}_0), \end{aligned} \quad (\text{A1})$$

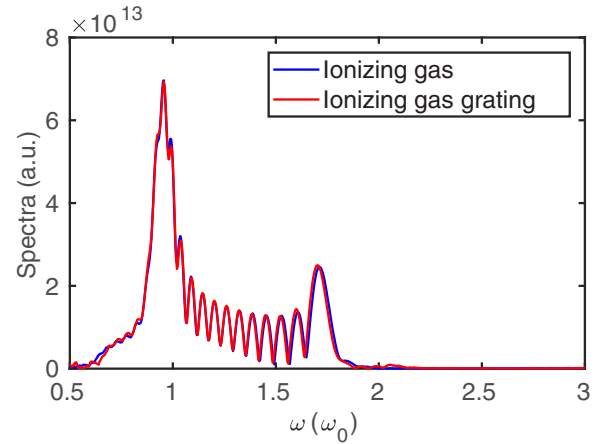


FIG. 5. PIC simulation of the laser spectra in the ionizing gas and gas grating at  $t = 200\lambda_0/c$ . The laser has a FWHM duration of 30 fs, a peak intensity of  $10^{15}$  W/cm<sup>2</sup>, and central wavelength of  $\lambda_0 = 1 \mu$ m. Both the background gas and gas grating have an average density of  $0.1n_c$ . The gas grating has a period of  $\Lambda \geq 0.8\lambda_0$  or  $\lambda \leq 0.3\lambda_0$ , and a modulation depth of  $0.05n_c$ .

where  $\mathbf{A}_0$  and  $\mathbf{A}$  are laser vector potentials of the pump and the driving pulse, respectively,  $c_s = \sqrt{ZT_e/m_i}$  is the ion acoustic velocity,  $Z$  is the plasma ion charge,  $T_e$  is the plasma temperature,  $e$  is the electron charge,  $m_{e(i)}$  is the electron (ion) mass,  $\delta n_e$  is the amplitude of electron density perturbation, and  $n_{e0}$  is the average electron density.

The laser electric field is  $\mathbf{E} = -\frac{1}{c} \frac{\partial \mathbf{A}}{\partial t}$ , and the 1-one-dimensional (1D) electric field can be written  $\mathbf{E}_0 = \frac{1}{2} E_0 \exp[-i(\omega_0 t - k_0 x) + \text{c.c.}]$  and  $\mathbf{E} = \frac{1}{2} E \exp[-i(\omega t + kx) + \text{c.c.}]$ , where  $\omega_0$  and  $k_0$  are the pump frequency and wave number, and  $\omega$  and  $k$  are the frequency and wave number of the driving pulse, respectively. By using the slowly varying envelope approximation, Eq. (A1) can be simplified to [57]

$$\begin{aligned} \frac{\partial E_0}{\partial t} - v_g \frac{\partial E_0}{\partial z} &= -i \frac{\omega_{pe}^2}{2\omega_0} E f^*, \\ \frac{\partial E}{\partial t} + v_g \frac{\partial E}{\partial z} &= -i \frac{\omega_{pe}^2}{2\omega_0} E f, \\ \left( \frac{\partial^2}{\partial t^2} - c_s^2 \frac{\partial^2}{\partial z^2} \right) f &= \frac{Ze^2}{4m_e m_i c^2} E_0 E^*, \end{aligned} \quad (\text{A2})$$

where  $\omega_{pe} = \sqrt{4\pi n_e e^2/m_e}$  is the plasma frequency,  $f \equiv \frac{\delta n_e}{n_{e0}}$  is the normalized plasma density, and  $k_B$  and  $\omega_B$  are the wave number and frequency of the ion acoustic wave.

In the limit of a low pump intensity below the ionization threshold and temporal scale of attoseconds, the influence of plasma grating from laser pulses can be neglected. Therefore, in the variable of  $\xi = z - v_g t$ , Eq. (A2) can be written as [40]

$$\begin{aligned} \frac{\partial E}{\partial t} &= -i \frac{\omega_{pe}^2}{2\omega_0} E_0 f e^{2i\omega_0 \delta N t}, \\ \times \frac{\partial E_0}{\partial t} + 2v_g \frac{\partial E_0}{\partial \xi} &= -i \frac{\omega_{pe}^2}{2\omega_0} E f e^{-2i\omega_0 \delta N t}, \end{aligned} \quad (\text{A3})$$

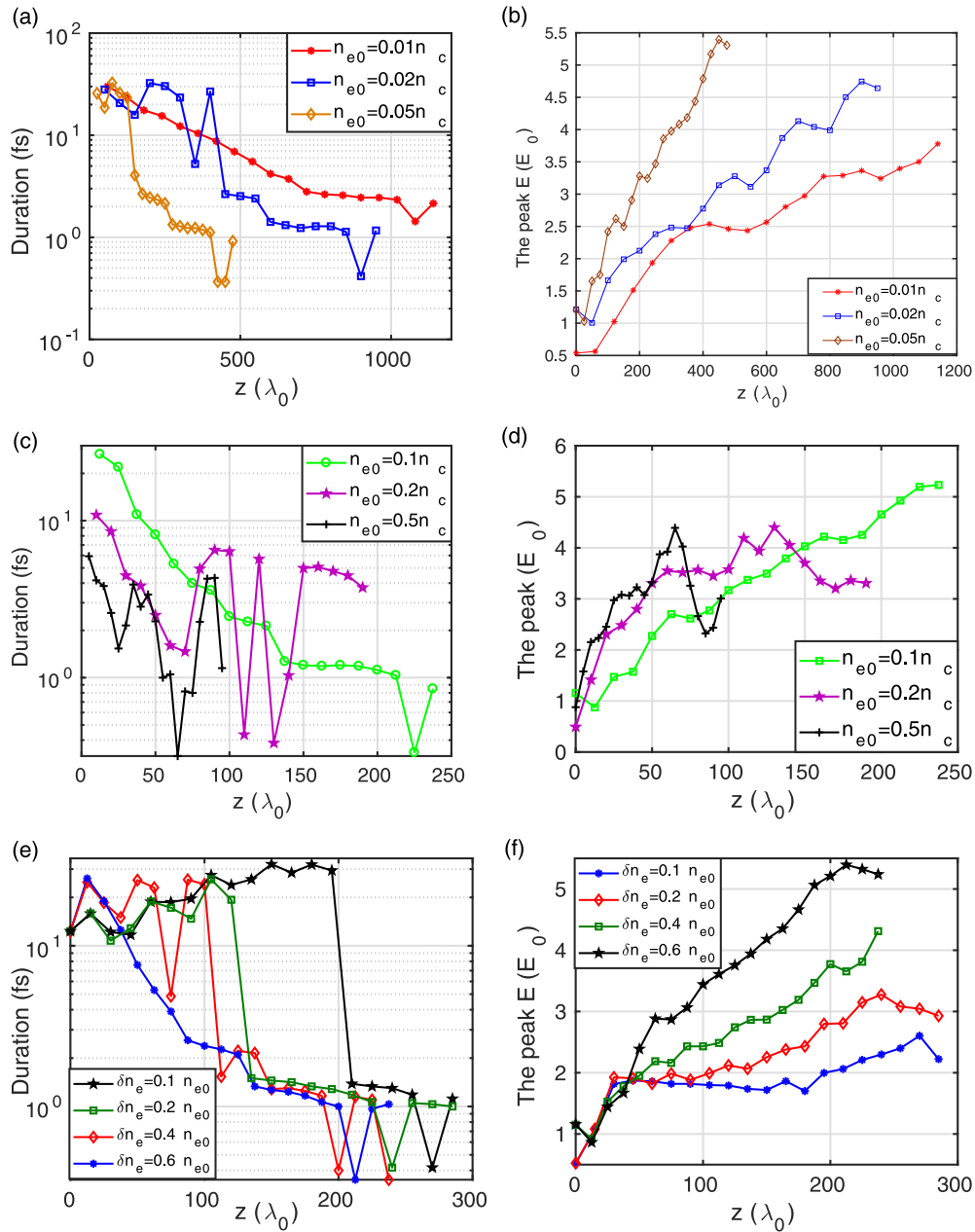


FIG. 6. 1D simulation of IAP generation at various plasma densities and FEPG modulation depths. Evolution of (a), (c) the FWHM duration and (b), (d) electric field of the driving pulse  $E$  at average plasma densities from  $0.01n_c$  to  $0.5n_c$ . Evolution of the FWHM duration (e) and  $E$  at different FEPG modulation depths.

where  $\delta N$  is the difference of refractive index between the point  $\xi$  and the resonant point  $\xi_0$ .

In a medium with a time-varying refractive index, the laser experiences a frequency shift while maintaining a constant wave vector in order to satisfy the dispersion relation [51]. Theoretical models have been developed to describe this phenomenon in ionizing plasma [48–50]. In the case of the gradient plasma grating, although the periodic structure also provides a time-varying refractive index, the integration over one period is close to zero. Consequently, the frequency upconversion effect resulting from the periodic structure can be neglected, allowing us to extend the existing theoretical models for the gradient FEPG. To validate this assumption, we

conducted particle-in-cell (PIC) simulations using the same laser pulse to ionize the gas and the gas grating. In the simulation, the grating period is set as  $\Lambda \geq 0.8\lambda_0$  or  $\Lambda \leq 0.3\lambda_0$  in case that the laser is reflected by the plasma grating, so both the laser pulses in the gas and gas grating can keep the same. The spectra were found to be nearly identical, as shown in Fig. 5, implying the upconversion effect is not impacted by the periodic structure of the plasma grating.

In variable  $\xi = z - v_g t$ , the upconverted light can be presented as [51]

$$\left( \frac{2}{v_g} \frac{\partial}{\partial \xi} - \frac{1}{v_g^2} \frac{\partial}{\partial t} \right) \frac{\partial}{\partial t} \mathbf{E} = \frac{\omega_{pe}}{v_g^2} \frac{n_e}{n_{e0}} \mathbf{E}. \quad (\text{A4})$$

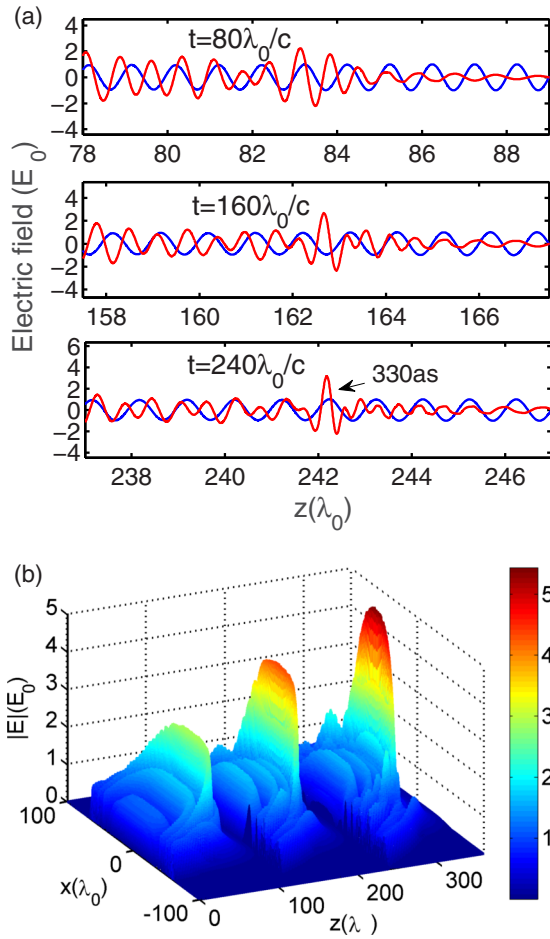


FIG. 7. (a) 1D waveforms of the driving pulse (red curves) and the pump (blue curves) at different interaction time. (b) 2D electric field of the driving pulse at different interaction time.

In general, the IAP can be obtained by numerically solving Eqs. (A3) and (A4). In the limit of a linear plasma gradient and  $\omega_{pe} \ll \omega$ , the second-order  $t$  derivative in Eq. (A4) can be neglected. Assuming the initial electric field is  $\mathbf{E} = E \exp(i\omega/\xi)$ , Eq. (A4) has an analytical solution of  $\frac{\omega_0}{\omega} E e^{i\omega t(\xi - \xi_0)}$  at  $-L < \xi < 0$ , where  $\omega = \omega_0(1 + ct\omega_{pe}^2/L\omega_0^2)^{1/2}$  is the shifted laser frequency [51].

For a laser induced plasma, a roughly linear density gradient can be formed in the pulse front. The upconverted light has an analytical solution of  $\frac{\omega_0}{\omega} E e^{i\omega t(\xi - \xi_0)}$  when  $\omega_{pe} \ll \omega$ , where  $\omega = \omega_0(1 + ct\omega_{pe}^2/L\omega_0^2)^{1/2}$  is the shifted laser frequency [51]. However, the upconverted process in PIG is more complex due the reflected pump. As the reflected pump is mainly affected by the plasma gradient and the propagation time, it can be approximately divided into a series of independent infinitesimal pulses. For  $dE$  at time  $t$ , the upconverted electric field at time  $t + \delta t$  can be described by Eq. (A5):

$$dE(t + \delta t) = \frac{\omega_0}{\omega_0(\delta t)} dE e^{i\omega(\delta t)(\xi - \xi_0)}. \quad (\text{A5})$$

As the resonant region in gradient FPEG is very narrow, the pump reflectivity is small and  $E_0$  is approximated to a constant

in Eq. (A3), so it is

$$dE = -i \frac{\omega_{pe}^2}{2\omega_0} E_0 f e^{2i\omega_0 \delta N t} dt. \quad (\text{A6})$$

Combing Eq. (A6) with Eq. (A5), the IAP has the following analytical solution:

$$E = \int_0^t i \frac{\omega_{pe}^2}{2\omega} E_0 f e^{2i\omega_0 \delta N t + i\omega(\xi - \xi_0)} dt. \quad (\text{A7})$$

## APPENDIX B: SUPPLEMENTAL PIC SIMULATION

The details of the simulation results with varying average densities and modulation depths are displayed in Fig. (6). As shown in Figs. 6(a) and 6(c), for  $n_{e0}$  from  $0.02n_c$  to  $0.5n_c$ , the full width at half maximum (FWHM) pulse duration is found to gradually decrease as the interaction length increases, reaching sub-500 attoseconds. After that, it does not further decrease but oscillates between  $\sim 1$  fs and hundreds of attoseconds. The oscillation has a period of about hundreds of femtoseconds, implying that it is mainly due to the plasma instabilities such as the fluctuations of the plasma density with a similar oscillation period, which makes the pump reflection not exactly overlap with the IAP peak when the pulse duration is too short. In the experiment, a proper interaction length can be set by adjusting the pump focal depth or the length of gas gratings. The required interaction length for IAP decreases with higher plasma density, attributed to a stronger upconversion effect at higher densities. The peak electric field of the driving pulse initially increases with plasma density, reaching a maximum value between  $4E_0$  and  $6E_0$  before saturating, as shown in Figs. 6(b) and 6(d). The conversion efficiency increased from 0.14% to 1.3% as the plasma density increased from  $0.02n_c$  to  $0.5n_c$ . However, for plasma densities above  $0.1n_c$ , both the electric field and pulse duration became unstable due to more serious plasma instabilities such as modulation instability [27,40] and group velocity dispersion, as shown in Fig. 6(c). Based on these results, a plasma density of  $0.1n_c$  was determined to be optimal for the IAP generation in the simulation. Moreover, for  $n_{e0} = 0.1n_c$ , the simulation results with the FEPG amplitudes from  $60\%n_{e0}$  to  $10\%n_{e0}$  are displayed in Figs. 6(e) and 6(f). The simulation results show that the peak electric field of the driving pulse decreases as the FEPG modulation depth decreases, and the required length of the plasma increases accordingly. However, the shortest pulse duration is little affected, and sub-500 attoseconds pulses can still be obtained at  $\delta n_e = 10\%n_{e0}$ . This suggests that the generation of IAPs is not strongly dependent on a large FEPG amplitude.

As the 3D simulation result is given in the main text, the 1D and 2D simulation results are supplemented here. The 1D simulation used a cell size of  $\Delta z = \lambda_0/200$ , and we found that decreasing the cell size to  $\lambda_0/1000$  did not significantly affect the results, indicating that this cell size is sufficient for accurately simulating the IAP generation. The waveforms of the driving pulse and pump at different times are shown in Fig. 7(a). The amplitude of the driving pulse gradually increases to about  $5.75E_0$  while the pulse duration decreases to 330 as. The pump waveform remains almost the same as it passes through the FEPG, implying a low reflectivity.

In the 2D simulation, the cell size was set to  $\Delta x \times \Delta z = \lambda_0/10 \times \lambda_0/200$ , with  $x$  and  $z$  representing the transverse and longitudinal directions, respectively. As shown in Fig. 7(b), while the beam size of the driving pulse tends to decrease as it grows, it maintains a high level of uniformity and quality.

A video named 1Dsimulation.avi is provided to show the dynamic process of how the IAP is formed in the 1D simulation. In the video, the green fringes are the background gas grating while the dark green fringes are the ionized plasma grating, the blue pulse is the pump, and the red pulse driving pulse.

- 
- [1] F. Calegari, G. Sansone, S. Stagira, C. Vozzi, and M. Nisoli, Advances in attosecond science, *J. Phys. B: At. Mol. Opt. Phys.* **49**, 062001 (2016).
- [2] M. Chini, K. Zhao, and Z. Chang, The generation, characterization and applications of broadband isolated attosecond pulses, *Nat. Photon.* **8**, 178 (2014).
- [3] M. Hentschel, R. Kienberger, C. Spielmann, G. A. Reider, N. Milosevic, T. Brabec, P. Corkum, U. Heinzmann, M. Drescher, and F. Krausz, Attosecond metrology, *Nature (London)* **414**, 509 (2001).
- [4] G. Sansone, E. Benedetti, F. Calegari, C. Vozzi, L. Avaldi, R. Flammini, L. Poletto, P. Villoresi, C. Altucci, R. Velotta, S. Stagira, S. D. Silvestri, and M. Nisoli, Single-cycle nonlinear optics, *Science* **314**, 443 (2006).
- [5] R. Kienberger, E. Goulielmakis, M. Uiberacker, A. Baltuska, V. Yakovlev, F. Bammer, A. Scrinzi, Th. Westerwalbesloh, U. Kleineberg, U. Heinzmann, M. Drescher, and F. Krausz, Atomic transient recorder, *Nature (London)* **427**, 817 (2004).
- [6] T. Gaumnitz, A. Jain, Y. Pertot, M. Huppert, I. Jordan, F. Ardana-Lamas, and H. Wörner, Streaking of 43-attosecond soft-x-ray pulses generated by a passively CEP-stable mid-infrared driver, *Opt. Express* **25**, 27506 (2017).
- [7] T. Witting, F. Frank, W. A. Okell, C. A. Arrell, J. P. Marangos, and J. W. G. Tisch, Sub-4-fs laser pulse characterization by spatially resolved spectral shearing interferometry and attosecond streaking, *J. Phys. B: At. Mol. Opt. Phys.* **45**, 074014 (2012).
- [8] P. B. Corkum, N. H. Burnett, and M. Y. Ivanov, Subfemtosecond pulses, *Opt. Lett.* **19**, 1870 (1994).
- [9] J. Li, X. Ren, Y. Yin, K. Zhao, A. Chew, Y. Cheng, E. Cunningham, Y. Wang, S. Hu, Y. Wu, M. Chini, and Z. Chang, 53-attosecond X-ray pulses reach the carbon K-edge, *Nat. Commun.* **8**, 186 (2017).
- [10] Z. Chang, Tsingle attosecond pulse and xuv supercontinuum in the high-order harmonic plateau, *Phys. Rev. A* **70**, 043802 (2004).
- [11] Z. Chang, Chirp of the single attosecond pulse generated by a polarization gating, *Phys. Rev. A* **71**, 023813 (2005).
- [12] I. J. Sola, E. Mével, L. Elouga, E. Constant, V. Strelkov, L. Poletto, P. Villoresi, E. Benedetti, J.-P. Caumes, S. Stagira, C. Vozzi, G. Sansone, and M. Nisoli, Controlling attosecond electron dynamics by phase-stabilized polarization gating, *Nat. Phys.* **2**, 319 (2006).
- [13] K. Zhao, Q. Zhang, M. Chini, Y. Wu, X. Wang, and Z. Chang, Tailoring a 67 attosecond pulse through advantageous phase-mismatch, *Opt. Lett.* **37**, 3891 (2012).
- [14] Z. Chang, Controlling attosecond pulse generation with a double optical gating, *Phys. Rev. A* **76**, 051403(R) (2007).
- [15] H. Mashiko, S. Gilbertson, C. Li, S. D. Khan, M. M. Shakya, E. Moon, and Z. Chang, Double optical gating of high-order harmonic generation with carrier-envelope phase stabilized lasers, *Phys. Rev. Lett.* **100**, 103906 (2008).
- [16] H. Vincenti and F. Quéré, Attosecond lighthouses: How to use spatiotemporally coupled light fields to generate isolated attosecond pulses, *Phys. Rev. Lett.* **108**, 113904 (2012).
- [17] K. T. Kim, C. Zhang, T. Ruchon, J.-F. Hergott, T. Auguste, D. M. Villeneuve, P. B. Corkum, and F. Quóró, Photonic streaking of attosecond pulse trains, *Nat. Photon.* **7**, 651 (2013).
- [18] C. M. Heyl, S. N. Bengtsson, S. Carlström, J. Mauritsson, C. L. Arnold, and A. L’Huillier, Noncollinear optical gating, *New J. Phys.* **16**, 052001 (2014).
- [19] S. Zhong, X. He, Y. Jiang, H. Teng, P. He, Y. Liu, K. Zhao, and Z. Wei, Noncollinear gating for high-flux isolated-attosecond-pulse generation, *Phys. Rev. A* **93**, 033854 (2016).
- [20] P. Tzallas, E. Skantzakis, C. Kalpouzos, E. P. Benis, G. D. Tsakiris, and D. Charalambidis, Generation of intense continuum extreme-ultraviolet radiation by many-cycle laser fields, *Nat. Phys.* **3**, 846 (2007).
- [21] X. Feng, S. Gilbertson, H. Mashiko, H. Wang, S. D. Khan, M. Chini, Y. Wu, K. Zhao, and Z. Chang, Generation of isolated attosecond pulses with 20 to 28 femtosecond lasers, *Phys. Rev. Lett.* **103**, 183901 (2009).
- [22] E. Skantzakis, P. Tzallas, J. Kruse, C. Kalpouzos, and D. Charalambidis, Coherent continuum extreme ultraviolet radiation in the sub-100-nm range generated by a high-power many-cycle laser field, *Opt. Lett.* **34**, 1732 (2009).
- [23] H. Mashiko, K. Oguri, and T. Sogawa, Attosecond pulse generation in carbon k-edge region (284 eV) with sub-250-pJ driving laser using generalized double optical gating method, *Appl. Phys. Lett.* **102**, 171111 (2013).
- [24] S.-W. Huang, G. Cirmi, J. Moses, K.-H. Hong, S. Bhardwaj, J. R. Birge, L.-J. Chen, E. Li, B. J. Eggleton, G. Cerullo, and F. X. Körtner, High-energy pulse synthesis with sub-cycle waveform control for strong-field physics, *Nat. Photonics* **5**, 475 (2011).
- [25] M. T. Hassan, T. T. Luu, A. Moulet, O. Raskazovskaya, P. Zhokhov, M. Garg, N. Karpowicz, V. Pervak, A. M. Zheltikov, F. Krausz, and E. Goulielmakis, Optical attosecond pulses and tracking the nonlinear response of bound electrons, *Nature (London)* **530**, 66 (2016).
- [26] G. M. Rossi, R. E. Mainz, Y. Yang, F. Scheiba, M. A. Silva-Toledo, S.-H. Chia, P. D. Keathley, S. Fang, O. D. Mücke, C. Manzoni, G. Cerullo, G. Cirmi, and F. X. Körtner, Sub-cycle millijoule-level parametric waveform synthesizer for attosecond science, *Nat. Photonics* **14**, 629 (2020).
- [27] V. M. Malkin, G. Shvets, and N. J. Fisch, Fast compression of laser beams to highly overcritical powers, *Phys. Rev. Lett.* **82**, 4448 (1999).
- [28] V. M. Malkin, G. Shvets, and N. J. Fisch, Detuned Raman amplification of short laser pulses in plasma, *Phys. Rev. Lett.* **84**, 1208 (2000).
- [29] R. M. G. M. Trines, F. Fiuza, R. Bingham, R. A. Fonseca, L. O. Silva, R. A. Cairns, and P. A. Norreys, Simulations of efficient



- raman amplification into the multipetawatt regime, *Nat. Phys.* **7**, 87 (2011).
- [30] Y. Ping, W. Cheng, S. Suckewer, D. S. Clark, and N. J. Fisch, Amplification of ultrashort laser pulses by a resonant raman scheme in a gas-jet plasma, *Phys. Rev. Lett.* **92**, 175007 (2004).
- [31] W. Cheng, Y. Avitzour, Y. Ping, S. Suckewer, N. J. Fisch, M. S. Hur, and J. S. Wurtele, Reaching the nonlinear regime of raman amplification of ultrashort laser pulses, *Phys. Rev. Lett.* **94**, 045003 (2005).
- [32] J. Ren, W. Cheng, S. Li, and S. Suckewer, A new method for generating ultraintense and ultrashort laser pulses, *Nat. Phys.* **3**, 732 (2007).
- [33] D. Turnbull, P. Franke, J. Katz, J. P. Palastro, I. A. Begishev, R. Boni, J. Bromage, A. L. Milder, J. L. Shaw, and D. H. Froula, Ionization waves of arbitrary velocity, *Phys. Rev. Lett.* **120**, 225001 (2018).
- [34] Z. Wu, Q. Chen, A. Morozov, and S. Suckewer, Stimulated raman backscattering amplification with a low-intensity pump, *Phys. Plasmas* **26**, 103111 (2019).
- [35] A. A. Andreev, C. Riconda, V. T. Tikhonchuk, and S. Weber, Single laser pulse compression via strongly coupled stimulated brillouin scattering in plasma, *Phys. Plasma* **13**, 053110 (2006).
- [36] S. Weber, C. Riconda, L. Lancia, J.-R. Marquès, G. A. Mourou, and J. Fuchs, Amplification of ultrashort laser pulses by brillouin backscattering in plasmas, *Phys. Rev. Lett.* **111**, 055004 (2013).
- [37] L. Lancia, J. R. Marquès, M. Nakatsutsumi, C. Riconda, S. Weber, S. Hüller, A. Mančić, P. Antici, V. T. Tikhonchuk, A. Héron, P. Audebert, and J. Fuchs, Experimental evidence of short light pulse amplification using strong-coupling stimulated brillouin scattering in the pump depletion regime, *Phys. Rev. Lett.* **104**, 025001 (2010).
- [38] L. Lancia, A. Giribono, L. Vassura, M. Chiamello, C. Riconda, S. Weber, A. Castan, A. Chatelain, A. Frank, T. Gangolf, M. N. Quinn, J. Fuchs, and J.-R. Marquès, Signatures of the self-similar regime of strongly coupled stimulated brillouin scattering for efficient short laser pulse amplification, *Phys. Rev. Lett.* **116**, 075001 (2016).
- [39] J.-R. Marqués, L. Lancia, T. Gangolf, M. Blecher, S. Bolanos, J. Fuchs, O. Willi, F. Amiranoff, R. L. Berger, M. Chiamello, S. Weber, and C. Riconda, Joule-level high-efficiency energy transfer to subpicosecond laser pulses by a plasma-based amplifier, *Phys. Rev. X* **9**, 021008 (2019).
- [40] Z. Wu, X. Zeng, Z. Li, Z. Zhang, X. Wang, B. Hu, X. Wang, J. Mu, J. Su, Q. Zhu, X. Wei, and Y. Zuo, Laser compression via fast-extending plasma gratings, *Matter Radiate Extreme* **7**, 064402 (2022).
- [41] Z. Li, Y. Zuo, X. Zeng, Z. Wu, X. Wang, X. Wang, J. Mu, and B. Hu, Ultra-intense few-cycle infrared laser generation by fast-extending plasma grating, *Matter Radiate Extreme* **8**, 014401 (2023).
- [42] M. Damzen, V. Vlad, V. Babin, and A. Mocofanescu, *Stimulated Brillouin Scattering Fundamentals and Applications* (Institute of Physics Publishing, London, 2003).
- [43] V. A. Gorbunov, S. B. Papernyi, V. F. Petrov, and V. R. Startsev, Time compression of pulses in the course of stimulated brillouin scattering in gase, *Sov. J. Quantum Electron.* **13**, 900 (1983).
- [44] F. Yang, F. Gygerand, and L. Thévenaz, Intense brillouin amplification in gas using hollow-core waveguides, *Nat. Photon.* **14**, 700 (2020).
- [45] I. D. Carr and D. C. Hanna, Performance of a Nd: YAG oscillator/amplifier with phase-conjugation via stimulated brillouin scattering, *Appl. Phys. B* **36**, 83 (1985).
- [46] H. Meng and H. J. Eichler, Nd: YAG laser with a phase-conjugating mirror based on stimulated brillouin scattering in sf6 gas, *Opt. Lett.* **16**, 569 (1991).
- [47] C. Zhang, Z. Nie, Y. Wu, M. Sinclair, C.-K. Huang, K. A. Marsh, and C. Joshi, Ionization induced plasma grating and its applications in strong-field ionization measurements, *Plasma Phys. Controlled Fusion* **63**, 095011 (2021).
- [48] K. Qu, Q. Jia, M. R. Edwards, and N. J. Fisch, Theory of electromagnetic wave frequency upconversion in dynamic media, *Phys. Rev. E* **98**, 023202 (2018).
- [49] K. Qu and N. J. Fisch, Creating localized plasma waves by ionization of doped semiconductors, *Phys. Rev. E* **99**, 063201 (2019).
- [50] A. J. Howard, D. Turnbull, A. S. Davies, P. Franke, D. H. Froula, and J. P. Palastro, Photon acceleration in a flying focus, *Phys. Rev. Lett.* **123**, 124801 (2019).
- [51] E. Esarey, G. Joyce, and P. Sprangle, Frequency up-shifting of laser pulses by copropagating ionization fronts, *Phys. Rev. A* **44**, 3908 (1991).
- [52] H. Peng, C. Riconda, S. Weber, C. T. Zhou, and S. C. Ruan, Frequency conversion of lasers in a dynamic plasma grating, *Phys. Rev. Appl.* **15**, 054053 (2021).
- [53] T. D. Arber, K. Bennett, C. S. Brady, A. Lawrence-Douglas, M. G. Ramsay, N. J. Sircombe, P. Gillies, R. G. Evans, H. Schmitz, A. R. Bell, and C. P. Ridgers, Contemporary particle-in-cell approach to laser-plasma modelling, *Plasma Phys. Control. Fusion* **57**, 113001 (2015).
- [54] M. Ammosov, N. Delone, and V. Krainov, Tunnel ionization of complex atoms and of atomic ions in an alternating electromagnetic field, *J. Exp. Theo. Phys.* **64**, 1991 (1986).
- [55] D. Strickland and G. Mourou, Chirped pulse amplification, *Opt. Commun.* **56**, 219 (1985).
- [56] G. A. Mourou, N. J. Fisch, V. M. Malkin, Z. Toroker, E. A. Khazanov, A. M. Sergeev, T. Tajima, and B. L. Garrec, Exawatt-zettawatt pulse generation and applications, *Opt. Commun.* **285**, 720 (2012).
- [57] W. L. Krueer, *The Physics of Laser Plasma Interaction* (Addison-Wesley, New York, 1988).